Ion-exchanged UPG-1 as a potential electrolyte for Fuel Cells

Pablo Salcedo-Abraira, Sérgio M F Vilela, Nieves Ureña, Fabrice Salles, Alejandro Várez, Patricia Horcajada

Ion-exchanged UPG-1 as a potential electrolyte for Fuel Cells

Pablo Salcedo-Abraira,[1] Sérgio M.F. Vilela,[1] Nieves Ureña,[2] Fabrice Salles,[3] Alejandro Várez,[2] Patricia Horcajada[1]**

[1] Advanced Porous Materials Unit (APMU), IMDEA Energy, Avda. Ramón de la Sagra 3, E-28935 Móstoles, Madrid, Spain

[2] Department of Materials Science and Engineering and Chemical Engineering, IAAB, Universidad Carlos III de Madrid, Avda. Universidad 30, E-28911 Leganés, Madrid, Spain

[3] ICGM, Univ. Montpellier, CNRS, ENSCM, 34095 Montpellier, France

KEYWORDS: Metal-Organic Frameworks, ionic exchange, proton conductivity, mixed matrix membrane.

ABSTRACT

Proton exchange membrane fuel cells (PEMFCs) are an attractive green technology for energy production. However, one of their mayor drawbacks is the instability of the electrolytes under working conditions (*i.e.,* temperature and humidity). Some Metal-Organic Frameworks (MOFs) have recently emerged as promising alternative electrolyte materials due to their higher stability

(compared with the organic polymers, currently used as electrolyte), proton conductivity and outstanding porosity and versatility. Here, we present the ionic exchange in a microporous zirconium phosphonate UPG-1 as an efficient strategy to enhance its conductivity and cyclability. Thus, labile protons of the hybrid structure were successfully replaced by different alkali cations (Li^+, Na^+ and K^+), leading to two magnitude orders higher proton conductivity than the pristine UPG-1 (up to $2.3 \cdot 10^{-2}$ $S \cdot cm^{-1}$, which is comparable with those of the commercial electrolytes). Further, proton conductivity was strongly influenced by the MOF hydrophilicity and the polarization strength of cation, as suggested by molecular simulation. Finally, a mixed matrix membrane containing the best performing material (the potassium exchanged one) was successfully prepared, showing moderate proton conductivity (up to 8.51 10^{-3} $S \cdot cm^{-1}$).

Introduction

The urgent fight against pollutants emission and global warming requires from the development of green technologies. Fuel cells (FCs) and, more precisely, proton exchange membrane fuel cells (PEMFCs), are an attractive technology to produce electricity by exclusively using carbon-free fuels (*e.g.* H_2).[1–3] A FC is basically constituted by an anode, a cathode, current collectors and an electrolyte. In brief, H_2 is oxidized into H^+ (in the anode), passing through the electrolyte to the cathode, where the reduction of O_2 into H_2O takes place. During this process, a current of e^- is generated from the cathode to the anode. The high specific energy and the generation of just water as sub-product make PEMFCs one of the most promising systems for electric vehicles.[4] Despite relevant advances in PEMFC components (*i.e.*, electrolyte, electrodes and current collectors),[5–7] the development of efficient electrolyte material is still a challenge,[8–12] due mainly to the instability under the operational conditions (temperature, humidity) of the current commercial

electrolytes (*i.e*. organic polymers such as Nafion®[13]).[14] In this line, an ideal electrolyte should present: i) a high proton conductivity (>10^{-2} S·cm^{-1}), which could be associated with the presence of a flexible hydrogen-bond network, the possibility of molecular reorientation and/or a driving force (usually a concentration gradient), insuring an efficient proton transport with a low activation energy (E_a); ii); a good thermal and chemical stability under the working conditions (temperature = 50-100ºC with relative humidity-RH% up to 95%); iii) chemical compatibility with the other FC components (*e.g.* electrodes); and iv) easy and low-cost scale-up and manufacturing as membranes.

Among the large variety of electrolyte materials (*e.g.,* polymers such as the benchmarked Nafion®,[13] zeolites,[15] perovskites,[16] polyoxometalates[17] or covalent organic frameworks),[18] metal-organic frameworks (MOFs) have been recently proposed as promising electrolytes in PEMFCs.[11,14,19–24] MOFs are porous crystalline hybrid materials built up from inorganic subunits (atoms, clusters, chains, etc) and organic polydentate linkers (carboxylates, azolates, phosphonates, etc) that combine an exceptional regular porosity (up to S_{BET} = 7800 $m^2 \cdot g^{-1}$) with a large chemical tuneability and structural versatility.[25,26] Three different strategies have been reported to synthesized either MOFs or MOF-composites with high proton conductivity,[27,28] including: i) intrinsically conductive MOF structures based on organic polycomplexant ligands bearing labile protons (phosphonate, sulfonate, carboxylate) functionalized or not with additional groups (*e.g.* -SO_3H, -NH_2, -OH, -CO_2H) able to modify the pK_a values of the material;[29–34] ii) the insertion within the MOF porosity of proton carrier species (*e.g.,* H_2SO_4, H_3PO_4, imidazole, 1*H*-1,2,4-triazole, lysine, ionic liquids);[24,35–41] and iii) the exchange of labile protons present in the structure by other cationic species (organic or inorganic), with the aim to enhance the proton conductivity.[42] Among the large panel of MOFs (1st strategy), phosphonate-based structures appear

to be excellent electrolyte candidates since they combine the presence of a larger number of labile protons (*vs.* carboxylate- or sulfonate-MOFs), associated with good conductivity, and with a higher stability.[43] Despite their *a priori* well-adapted properties, phosphonate-MOFs (P-MOFs) have been less explored as proton conductors than the carboxylate-based ones. The low commercial availability and poor solubility of the ligands, together with their difficult structural elucidation have limited the number of available P-MOFs (P-MOFs vs. carboxylate-MOFs ≈ 1:12; according to Web of Science). Further, the *de novo* synthesis approach often requires of time-consuming trial-and-error process, making more attractive (faster and easier) the two other post-synthetic strategies. In this sense, many guest molecules have been encapsulated into MOFs to enhance the proton conductivity of materials (2nd strategy). In contrast, to the best of our knowledge, there is only one report dealing with the 3rd ionic-exchange strategy. This recent work presents a new rare earth-based phosphonate MOF and its post-synthetic modification by exchanging labile H^+ by K^+ (denoted 1K_Eu), leading to an remarkable increase on its proton conductivity (from $1.24 \cdot 10^{-5}$ to $1.89 \cdot 10^{-1}$ $S \cdot cm^{-1}$ at 94 ºC and 98% RH) and confirming this approach as highly promising.[42] However, the toxicity and cost of rare earth precursors (2.4 and 20 k€ *per* kg for the Y and Eu salt, respectively; intraperitoneal lethal dose-LD_{50} (guinea pig) YCl_3= 85 $mg \cdot kg^{-1}$) strongly limit the use of 1K_Eu material at industrial scale.

Manufacturing MOFs as MMMs by using different polymers is a commonly applied method for different applications.[44–46] In particular, the specific shaping of the conducting materials into membranes is a crucial step to integrate the electrolyte into the final PEMFC device, allowing the transport of the H^+ through the membrane from the anode to the cathode. There are some examples in the literature reporting the use of a MMMs incorporating pure MOFs[47–49] and guest@MOF composites[50] as electrolyte for PEMFCs, exhibiting in all the cases promising conductivity values

(up to $2.3 \cdot 10^{-2}$ S·cm^{-1} for a NH_3@Zn-MOF composite in a Nafion-based membrane).[50] However, and even though the relevance of this topic, no MMMs containing P-MOFs have been described so far.

Taking into account the above mentioned, we present here the post-synthetic modification by ionic exchange of the robust microporous zirconium phosphonate UPG-1 (UPG stands for University of Perugia).[51] UPG-1 or $Zr[H_4ttbmp]_2 \cdot 10H_2O$ (H_6ttbmp = 2,4,6-tris(4-(phosphonomethyl)phenyl)-1,3,5-triazine) was selected since: i) its recently proven proton conductivity ($5.1 \cdot 10^{-4}$ S·cm^{-1}),[24] associated to its trigonal structure based on 1D chains of Zr(IV) octahedra connected by PO_3C tetrahedra from the ligand, which exhibits one uncoordinated -PO_3H_2 and two coordinated -PO_3H groups, leading to eight uncoordinated –OH moieties *per* unit formula that establish efficient proton conducting pathways; ii) high thermal, chemical and mechanical stability (up to 450 ºC, in aqueous solution and under pressure) compatible with the PEMFCs operational conditions; iii) its high 1D porosity with diameters of 5 and 10 Å allows a good proton transport, as well as the insertion of additional proton carriers (*e.g.*, water, lysine) and; iv) the low toxic and cost of the UPG-1 components. In this line, we have recently reported the insertion of the proton carrier amino acid lysine into UPG-1 porosity as an easy way to improve its proton cyclability, although not the intrinsic proton conductivity.[24] Thus, we propose here to go a step further, not only enhancing the material cyclability, but also improving the proton conductive properties of UPG-1 by replacing labile protons of the ligand by alkali cations (*i.e.* Li^+, Na^+, K^+). Thus, both experimental and simulation techniques were applied in an attempt to understand the conductive properties of the solids. The best performing MOF sample in terms of conductivity ($2.3 \cdot 10^{-2}$ S·cm^{-1}) was finally shaped as an proton conductive MMM using a sulfonated polysulfone (SPSU) polymer, characterizing both their thermal stability by TGA and proton conductive properties by IS. The

sulfonate polysulfone polymer (SPSU) was selected as a polymeric support due to its polymeric hydrophilic nature, its proton conductivity, and its previously reported shaping into membranes.[52]

Experimental Methods

Synthetic Procedure:

Synthesis of [Zr(H_4ttbmp)$_2$]·10H_2O (UPG-1):

UPG-1 as well as its corresponding organic linker (*i.e.,* 2,4,6-tris[4-(phosphonomethyl)phenyl]-1,3,5-triazine; H_6ttbmp) were synthesized according to the reported procedure with slight modifications.[24] Briefly, $ZrOCl_2 \cdot 8H_2O$ (0.2852 g, 0.887 mmol) was dissolved in 16.1 mL of a 2.9 M HF solution in a 103 mL Teflon-lined autoclave reactor. Then, to this solution, 11.5 mL of methanol, 23 mL of distilled water and 0.5428 g of H_6ttbmp (0.918 mmol) were added. The reactive mixture was stirred at ambient temperature for 5 min and then, transferred to an oven where the reaction took place at 80 ºC for 48 h. The resulting white powder was first washed with distilled water, then with a distilled water/methanol (3:1) mixture and finally with methanol, collecting the solid by filtration and drying at ambient temperature.

Ionic Exchange:

For all the samples the experimental procedure was the same. 300 mg (0.2364 mmol) of activated UPG-1 (150 ºC under primary vacuum for 5 h) were suspended in 47.28 mL of a 0.05M ethanolic solution of MOH (M = Li, Na, K; 10 eq.). The suspensions were stirred (400 rpm) at room

temperature for 48h. Then, the exchanged samples were recovered by filtration, washed with ethanol and dried under air. Yield = 90%

Synthesis of Sulfonated Polysulfone:

SPSU was synthesized according to published data[53] and Fig. S1. Briefly, polysulfone Udel® (PSU, 22000 g mol^{-1}, 5,00 g) was dissolved in 1,2-dichloroethane (DCE, 30 mL) under inert atmosphere at ambient temperature. Subsequently, the sulfonating agent (trimethylsilyl chlorosulfonate-TMSC, previously dissolved in DCE) was added dropwise and maintained for 24 h (PSU:TMSCS molar ratio 1:1). Sulfonation reaction of PSU was performed using TMSCS since a previous work reported a lower degradation of the polymer chains.[52] The resulting polymer was precipitated in a 0.1 M solution of NaOH and dried under vacuum at 60 ºC. Then, the polymer was immersed in a 1 M HCl solution at 60 ºC for 24 h to replace Na^+ by H^+.

Membrane Preparation:

SPSU (0.9 g) and K@UPG-1 (2 wt.%) were dissolved in 12 mL of N,N-dimethylformamide (DMF) under stirring for 24 h at room temperature. The mixture was filtered and, finally, casted onto a flat glass plate and dried in an oven to obtain the membrane. The thickness of the resulting membranes (denoted as K@UPG-1_SPSU) was around 50 μm (as determined by SEM).

General Instrumentation:

Powder X-ray diffraction (PXRD) patterns were collected from 3 to 35° (2θ) using a step size of 0.02° and 2.5 s per step in continuous mode in an Empyream PANALYTICAL diffractometer,

equipped with a PIXcel3D detector and with a copper radiation source (Cu Kα, λ =1.5406 Å), operating at 45 kV and 40 mA. Thermogravimetric analysis (TGA) of M@UPG-1 powders were carried out using a SDT Q-600 thermobalance (TA instruments) under air flow (100 mL min^{-1}) with a heating rate of 5 °C min^{-1} between room temperature and 800 °C. In the case of SPSU a Pyris TGA1 instrument from Perkin-Elmer was used and the experiments were carried out under air atmosphere at a rate of 10 °C min^{-1} heating from 40 to 600 °C. Fourier transformed infrared (FTIR) spectra were collected in the 4000 to 400 cm^{-1} range using a Thermo Nicolet 6700 FTIR with attenuated total reflectance (ATR) accessory instrument (Thermo scientific, USA). Elemental analyses from light elements were carried out in a Flash 2000 analyzer from Thermo Scientific. Zr, P, Li, Na and K were measured by induced coupled plasma atomic emission spectroscopy (ICP-OES) using a 2300DV spectrometer from PerkinElmer. X-ray energy dispersive spectroscopy (XEDS) measurements of the pellets were carried out in a Hitachi TM-1000 tabletop SEM. The morphology of membranes was characterized by field emission scanning electron microscopy (FE-SEM) using a FEI TENEO-LoVac equipped with an energy-dispersive detector (EDS-EDAX). SEM images were recorded operating at 5-10 kV. Polymers were analyzed by proton nuclear magnetic resonance spectroscopy (^{1}H-NMR). Spectra were registered at 300 MHz on a Bruker Avance DPX-300 spectrometer using DMF-d_7 and dimethyl sulfoxide (DMSO-d_6) as the solvents. TMS was used as the internal reference.

Proton Conductivity:

Proton conductivities (σ) of M@UPG-1 and membranes was investigated by impedance spectroscopy (IS). M@UPG-1 was prepared on compacted pellets of crystalline powders (uniaxial

pressure = 49 MPa and then, isostatic pressure = 60 MPa; ~6 mm diameter) sputtered with gold (by sputtering in a Leica EM ACE 200 instrument) to make the ion-blocking electrodes. Their apparent densities were calculated, taking into account their weight and geometric dimensions (*i.e.*, diameter and thickness). The electrical measurements of the MOF were performed on a parallel-plate capacitor configuration under air atmosphere. Measurements were carried out using an Impedance/Gain-Phase Analyzer SI 1260 (Solartron, UK), applying a 100 mV amplitude signal in the in the 10^{-1}–10^{7} Hz frequency range. For the membrane's electrochemical characterization, proton conductivity was measured using, additionally to the impedance analyzer, an interface (Solartron 1287). Measurements were carried out in the range of frequency from 10^{-1} to 10^{6} Hz applying 10 mV amplitude sinusoidal wave perturbation. Measurements at different temperatures (30–90 °C) and relative humidity values (RH) of 70 and 90% were performed in a programmable climatic chamber (BINDER, UK). In order to ensure the reproducibility of all measurements, a dwell time of 15 min was defined for the system to reach stable conditions. By using this method, the RH and temperature could be controlled up to ±1 % and ±1 °C, respectively. Measurements were carried out in the range of frequency from 10^{-1} to 10^{6} Hz applying 10 mV amplitude sinusoidal wave perturbation. Measurements at temperature range (from 40 to 90 °C) at 90% RH were performed. Impedance data analysis was performed using the ZView2 program.[54]

The σ (in S cm^{-1}) was calculated by the following equation (Equation 1):

$$\sigma = \frac{l}{R \text{ X } A}, \qquad (1)$$

where l and A are the thickness (cm) and the area (cm^2) of the pellets, respectively. R is the ohmic resistance (Ohm) obtained from the intersection of the in Nyquist plot of the impedance curve with axis of the real component of the impedance.

The activation energy was estimated using the following equation (Equation 2), employed for non-Arrhenius polymeric ion conductors

$$\sigma = \sigma_o * exp\left(\frac{-E_a^{VTF})}{K(T-T_0)}\right), \quad (2)$$

where σ_0 is the prefactor, T is the absolute temperature, k is the Boltzmann constant, E_a^{VFT} is the pseudoactivation energy and T_0 is related in polymers to glass transition temperature at which the "free" volume disappears or at which configuration free entropy becomes zero. This system could be also related to that temperature in which molecular water motions cease.

Molecular Simulations:

In order to determine the organization of the water molecules and alkali cations in the structure, Monte Carlo simulations were performed. Prior to these calculations, the UPG-1 structures have been built by considering the experimental dry structure[24] in which some cations replace hydrogen (by taking into account the experimental content). Then, three models were obtained with charges depending on the nature (and therefore the amount) of the compensating cations (*i.e.* Li^+, Na^+ and K^+). Partial charges (Fig. S2-4) for the different solids were extracted using the qEq methodology based on electronegativity equalization approach and then combined with Universal Force Field (UFF)[55] for Lennard Jones parameters for solids and mixed with TIP4P-2005[56] for water molecules. Regarding the cations, the partial charges were fixed at +1 and UFF force field was also used for Lennard Jones parameters. Then, configurations were extracted from Monte Carlo calculations performed at P/P_0=1 (where P_0 is the liquefaction pressure for water). Monte Carlo calculations[57] were then performed at 300 K to determine the saturation loading in water molecules inside the UPG-1 structures containing the different cations and to extract the plausible

configurations of water clusters inside the pores. 100×10^6 steps for equilibration and 10×10^6 steps of production were considered. The electrostatic interactions were calculated by Ewald summation, while the short-range contributions corresponding to Lennard Jones parameters were computed by applying the Lorentz-Berthelot rules applied on UFF force field parameters for UPG-1 atoms. The simulations were conducted using the different simulated structures considering multicells (corresponding to 1x1x6 unit cells), which is consistent with a cut-off distance for Lennard Jones interactions equal to 12 Å.

Results and Discussion:

The labile protons of the UPG-1 material were successfully replaced by Li^+, Na^+ or K^+ using a simple and efficient impregnation method, suspending the pristine powdered material in different ethanolic solutions of the corresponding metal hydroxides (Scheme 1). The UPG-1 structure was preserved in all the cases, as supported by PXRD (Fig. S5). Upon the cation exchange, the intensity of some reflections is nevertheless modified, which may be related with the different pore content due to the presence of the cations. Note here that the cation exchanged samples did not show any accessible porosity to N_2, as previously reported for the pristine UPG-1 due to a low affinity for the adsorbent.[51]

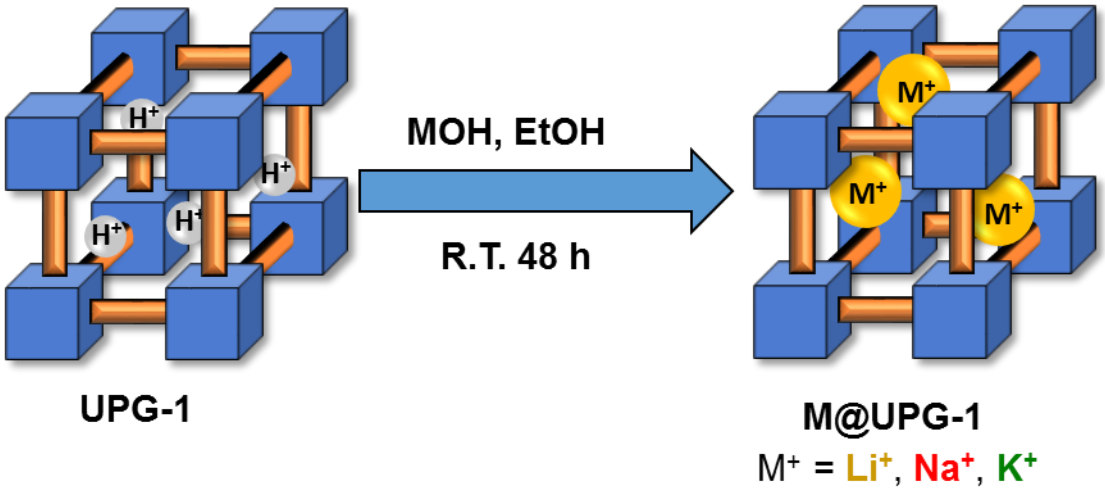

Scheme 1: Synthetic procedure of the ionic exchanged UPG-1 samples

Table 1: Experimental molecular formula for the ion exchanged samples together with the water adsorption enthalpy and water content estimated from molecular simulations.

Material	Experimental		Simulated data*	
	Formula	Water molecules *per* m.c.**	Water molecules *per* m.c.**	Water adsorption enthalpy ($kJ \cdot mol^{-1}$)*
Li@UPG-1	$Li_{4.88}@Zr(H_{1.76}ttbmp)_{2.16}$	934	940	-130
Na@UPG-1	$Na_{5.58}@Zr(H_{1.21}ttbmp)_{1.95}$	940	912	-130
K@UPG-1	$K_{4.78}@Zr(H_{1.61}ttbmp)_{2.12}$	1062	840	-104

*Calculated from Monte Carlo simulations. **m.c. corresponds to a multi-cell of 1x1x6 u.c. used for simulation.

Extracted from the elemental composition analysis (ICP-OES Zr, P and Li/Na/K), a partial exchange of the H^+ from the free phosphonic acid groups of the material was calculated (around 5 over the 8 available protons were replaced, Table 1). Considering these experimental values, molecular calculations were carried out to gain some insights about the potential interactions between the cations and the hybrid network (Figs. S6-8). From simulation, the main interactions are established between the phosphonic group and the benzene rings of the MOF and the

monovalent cations. In agreement to this, FTIR spectra (Fig. S9) present a shift to lower wavenumber of some stretching bands (P=O and P-O at around 1250 and 1182 cm^{-1}), being more important with the mass increasing of the exchanged cation (Li<Na<K, Fig. S9). For instance, in the case of K@UPG-1 sample, the band at 1250 cm^{-1} was shifted up to 1240 cm^{-1}. The effect of the effective ionic exchange can be also evidenced in other less affected spectroscopic bands, that correspond to the vibrations of the aromatic rings from the MOF linker (between 1625 and 1500 cm^{-1}).

Considering the strong impact of the water content on the final ion conductivity, the influence of the cation exchange on the water adsorption in UPG-1 was evaluated by both experimental (TGA) and simulation (Monte Carlo) techniques (Table 1). Prior to the TGA, the samples were kept under a controlled atmosphere (RH = 70% overnight) in order to homogenize and compare the exchanged UPG-1 solids. Thus, the ionic exchanged samples present a higher water content than the pristine UPG-1 (780 water molecules in the multicell-m.c. for the UPG-1 calculated by TGA, see Table 1 and Fig. S10). These values of the exchanged solids were compared with those obtained from simulation at saturation, being in very good agreement, except for K@UPG-1. The slightly higher experimental amount of water (*vs*. simulation) could be explained by the different considered conditions (*i.e.* saturation in simulation and 70% RH in experiments). Thus, one could hypothesize a complete saturation of the pores in K@UPG-1 at 70% RH, being the water excess probably located on the particles outer surface. In addition, only one configuration of the K^+ distribution has been investigated by molecular simulations, impacting on the hydration around the cations. Further, it should be mentioned that the two types of pores (5 and 10 Å; Fig. S11) present in the UPG-1 possess a different hydration behavior,[24] probably also affecting the cation location and material hydration.

Considering the already proven proton conductivity of the UPG-1 ($5.1 \cdot 10^{-4}$ $S \cdot cm^{-1}$ at 90% RH and 70 ºC),[24] the exchanged materials were tested as protonic conductors. After press-molding the powdered samples as 6 mm-diameter cylindrical-like pellets, their crystalline structural integrity was confirmed by PXRD (Fig. S12) and their protonic conductivity tested by impedance spectroscopy under different conditions of temperature and RH (see Experimental Methods for further details). For RH < 50% the conductivity is less than 10^{-6} $S \cdot cm^{-1}$ and measurements are unstable over the whole frequency range. For all the samples, the conductivity increases with the increasing of RH. The results further revealed the importance of water molecules as proton carriers in proton conductivity. Typical impedance datasets of the Na@UPG-1 sample are displayed in the Figure 1. At high frequency, the data show a slightly distorted semicircle with an associated capacitance of 6.5 $pF \cdot cm^{-1}$ that was, therefore, attributed to the bulk resistance of the sample. Also, an inclined spike with an associated capacitance of 0.2 $\mu F \cdot cm^{-1}$ can be observed in the low frequency region, which indicates a partial-blocking electrode response consistent with proton migration. There are two defined regions in the frequency dependent conductivity (the plateau at high frequencies and the dispersion at low frequencies). The plateau corresponds to constant conductivity associated with the bulk conductivity of the sample, as extracted from the intersection of the semicircle in the Z' axis of the Nyquist plots at low frequencies. Similar behavior is observed for the rest of cation exchanged samples, although the conductivity values slightly changes from one sample to another. The one with the highest conductivity is K sample while the Li sample has the lowest value.

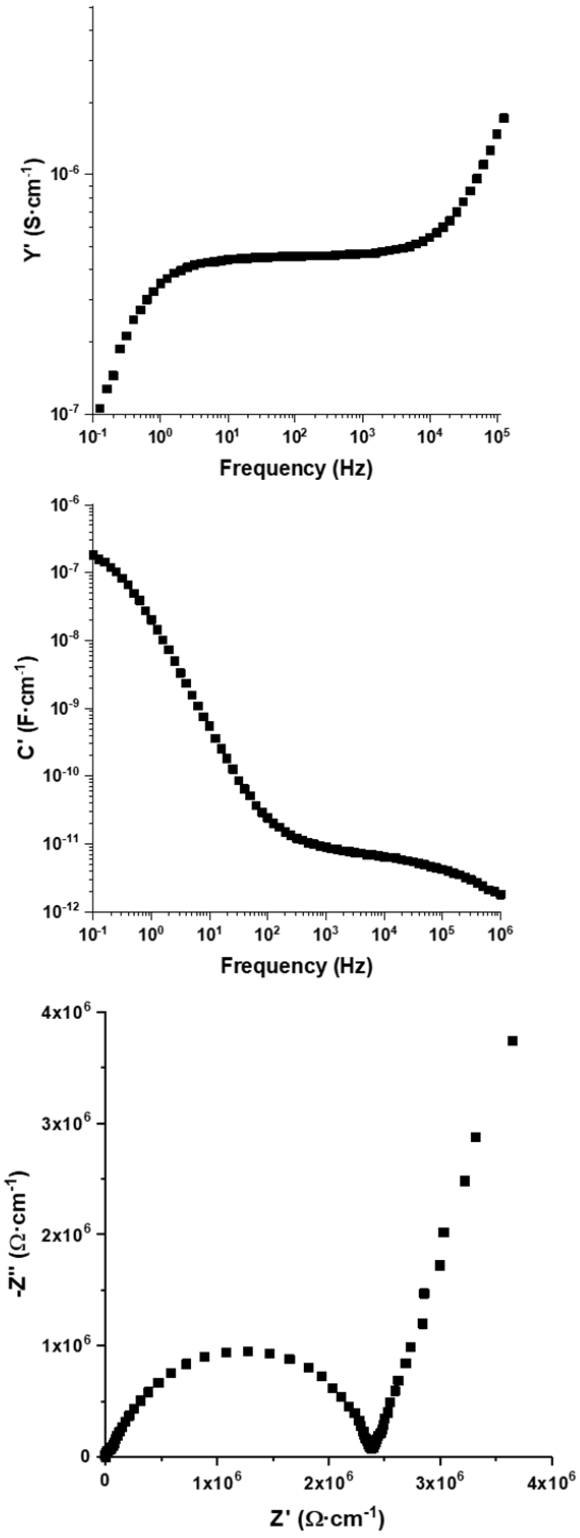

Figure 1: Impedance data set of Na@UPG-1 at 70% RH and 30 ºC

As expected, the conductivity is strongly dependent on temperature (Fig S13-S16) and RH (Fig S17) for all the samples. In Figure 2 the evolution of conductivity with the temperature for the three exchange samples is displayed, summarizing the above results. At 70% RH, the Nyquist plots from the show a single semicircle, attributed to the bulk resistance of the solids. Additionally, at temperatures higher than 60ºC, a second depressed semicircle appears in the K@UPG-1 sample at intermediate frequencies, overlapping with a third one at lower frequencies (Fig. S18). When increasing the RH to 90%, the plots significantly change, showing one depressed semicircle that is not completely closed at higher frequencies. Also, a second depressed semicircle appears at intermediate frequencies for the Na and K samples, overlapping with a third one at lower frequencies (Figs. S15-16). This new contribution (at 90% RH for Na and at both 70 and 90% RH for the K) could be associated to an extrinsic transport through MOF intergrain region, as previously described by Tominaka and Cheetham.[58] These observations suggest an extrinsic contribution from the water on the interparticle surface, and not only an intrinsic one corresponding to the protons of the framework and/or in the micropores; also supporting the previous hypothesis concerning the presence of water on the K@UPG-1 surface (TGA data Table 1). In general, the proton conductivity increases around one order of magnitude when passing from 70 to 90% RH (Table S1 and Fig. S12). Interestingly, the exchanged samples showed a conductivity significantly higher than the pristine UPG-1, reaching up to 2 orders of magnitude higher values (*i.e.* from the $5.1 \cdot 10^{-4}$ $S \cdot cm^{-1}$ magnitude previously reported for UPG-1[24] to $2.3 \cdot 10^{-2}$ $S \cdot cm^{-1}$ for K@UPG-1 at 90% RH and 90 ºC). Although the Li and Na samples also led to enhanced proton conductivities ($2.65 \cdot 10^{-3}$ and $9.57 \cdot 10^{-3}$ $S \cdot cm^{-1}$, respectively), K@UPG-1 was the best performing solid. This could be rationalized by considering that the proton conductivity is related with the water content and its mobility. The higher water amount of the exchanged samples compared to the pristine

UPG-1 (Table 1) might justify the higher conductivity values reached for the M@UPG-1 samples. On the other hand, and according with the polarization strength of the different cations ($Li^+ > Na^+ > K^+$), the solvation state of the different cations in the MOF was estimated by Monte Carlo simulation. The lower solvation state (840 water molecules *per* m.c., Table 1) of K@UPG-1 compared to the Li and Na solids (940 and 912 water molecules *per* m.c., respectively, Table 1) might favor a higher water mobility, also supporting the best proton conductivity of K sample. In addition, considering a single configuration of the cations location, it was observed that the K^+ cations are more affected by the hydration. Indeed, more K cations are less interacting with the framework at the hydrated state compared to the dry state (see Fig. S8; shorter distances highlighted in pink). This suggests that hydration favors the cations location in the center of pores, enhancing the proton conductivity. Such a behavior is less evidenced in the simulations performed for Li and Na@UPG-1 (see Fig. S6 and S7).

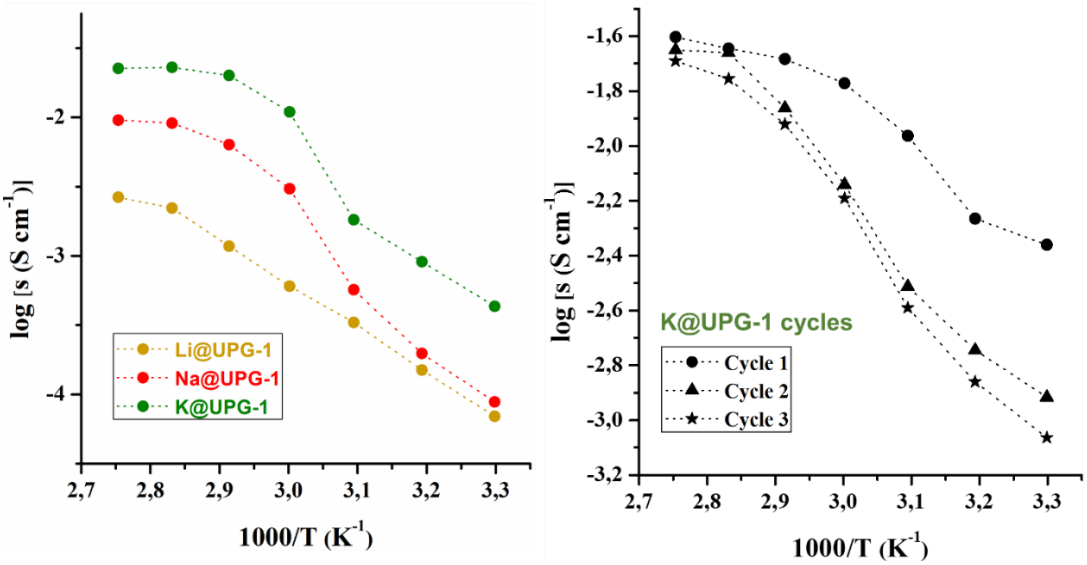

Figure 2: Evolution of conductivity with temperature for the three exchanged samples (left) and for the K@UPG-1 after different cycles at 90% RH.

Additionally, the hydrophobic/hydrophilic balance of the materials, impacting on the proton conductive pathways,[24] was assessed by theoretically estimating the water adsorption enthalpies. Considering the liquefaction enthalpy of water (-40 kJ·mol^{-1}), all the modified materials can be considered as hydrophilic (ΔH_{ads} > -40 kJ·mol^{-1}, Table 1), in contrast with the hydrophobic character of the pristine UPG-1 (ΔH_{ads} = -23.8 kJ·mol^{-1}). In the case of the UPG-1, it was found that the proton conductive pathways were mainly based on the H-bonds existing between the water molecules preferentially located in the large pores (10 Å), being the framework not strongly involved in the conduction process.[24] In contrast, for the exchanged samples (extracted from the GCMC simulations, Fig. S19-21), the water molecules are present in both pores of the structure (5 and 10 Å), interacting with both the cations and other water molecules (Fig. S22-24), establishing more efficient proton conductive pathways along the 1D channels. Conductive pathways can be determined from snapshots extracted from Monte Carlo simulations and they illustrate the implications of both cations and water molecules in the diffusion mechanisms (Fig S21-S23) as represented by interaction distances ranging around 2 Å. Such a combination of charge carriers can explain the enhancement of the conductivity measurements. As previously mentioned, the fact that the cations K^+ are less polarizing compared to Li^+ and Na^+ can justify higher experimental conductivity measurements. In addition, one could suggest that the ionic conductivity is here mainly dominated by the proton conduction, as supported i) the large number of proton carriers (water molecules) when compared with the inserted cations (water:cation ratio 4:1; Table 1), ii) the increase of the conductivity with the RH%; and iii) preliminary molecular dynamics simulations, showing that the diffusion of the extra-framework cations is slightly limited to close environments.

In order to shed some light to the ion conduction mechanism, the activation energy of the process was estimated. From the Figure 2, it is clear that the samples do not present an Arrhenius behavior. Pseudo-activation energies (E_a) were calculated by fitting the conductivity data to the Vogel-Tamman-Fulcher (VTF) equation (Fig. S25),[59] a widely use approximation for non-Arrhenius polymeric ion conductors.[60] Although not fully understood yet, this non-Arrhenius behavior has been already described for other MOF structures.[61,62] The obtained values of the pseudo-activation energies from the VTF adjustment (Table S2) were in the range attributed to a Grotthuss mechanism (charge carrier transported by water molecules; <0.5 eV),[63] which involves proton mobility through H-bonding from one carrier to another with a reorientation between one carrier and the next one.[61,64] The slightly higher E_a values in the exchanged samples compared to the pristine one (0.02 eV)[24] could be explained by the presence of the cations within the pores, interacting with the water molecules. Between the samples, the tendency of the E_a might be related with the solvation degree of each cation (similarly than previously discussed for the conductivity, Table 1), where the less solvated cation is associated with the lower E_a.

One could also compare the here obtained values of conductivity with those of other pure phosphonate-based MOFs (Table S3). P-MOFs usually present conductivity values ranging from 10^{-6} to 10^{-3} S·cm^{-1}.[24,42,65–70] Only three P-MOF structures exhibit similar (PCMOF2$_{1/2}$[71]; 10^{-2} S·cm^{-1}) or slightly higher (1K_Eu[42] and $Gd_2(H_3nmp)_2$;[72] 10^{-1} S·cm^{-1}) conductivity values than K@UPG-1 (10^{-2} S·cm^{-1}). However, the PCMOF2$_{1/2}$ and 1K_Eu solids did not present any cyclability features, and the structural integrity of the 1K_Eu was not evaluated. Also, the K-exchanged 1K_Eu and the $Gd_2(H_3nmp)_2$ present a higher cost and toxic character, making K@UPG-1 a very promising green, cheaper and efficient proton conductor. Finally, considering the best conductivity values of the K@UPG-1, cyclability tests were carried out to evaluate its stability under the best

working conditions (RH = 90%). Upon three cycles at 90 ºC (Table S4), the K@UPG-1 not only kept intact its proton conductivity but also retained its crystalline structure (evaluated by PXRD, Fig. S26) and composition (analyzed by SEM-EDX, Table S5) up to six cycles. Additionally, the thermal stability of the K@UPG-1 crystalline structure has been evaluated by PXRD, evidencing that the structure was perfectly kept up to 100 ºC, similarly to the original UPG-1 material (Fig. S27).

With the aim to improve the mechanical stability of the future electrolyte material while adapting it to a future practical FC device, a MMM was prepared based on a SPSU 2 wt.% containing K@UPG-1 (denoted as K@UPG-1_SPSU). The homogeneous distribution of the MOF particles within the MMM (~50 μm-thickness) was confirmed by SEM (see both flat and transversal views of the membrane; Figures 3 and S28). The sulfonation reaction of PSU was successfully confirmed by means of ^{1}H-NMR spectroscopy (Fig. S29). Comparing the ^{1}H-NMR spectra of PSU and SPSU in the range of chemical shifts corresponding to the aromatic protons (6.40 ppm δ < 8.40 ppm), SPSU showed a shift (δ = 7.71 ppm, Fig. S29b) of the peak associated with the H4' protons, which were adjacent to the attached sulfonic groups.[49] The degree of sulfonation (DS), estimated using the Kopf equation,[53] was 100% (*i.e.,* the polymer presents one sulfonic group *per* monomer). This fact might ensure a high contribution of the SPSU on the final proton conductivity of the MMM. TGA of SPSU (Fig. S30) shows three different of weight losses. The first one, between 50and 250 ºC, was related to the departure of the adsorbed water. The second step, between 250and 450 ºC, was attributed to the sulfonic groups decomposition. The third thermal degradation, above 450 ºC, was assigned to the degradation of the polymeric backbone. Thus, the thermal stability of the polymer was estimated to around 250ºC, being largely above the temperatures used on the conductivity measurements (100 ºC under air atmosphere).

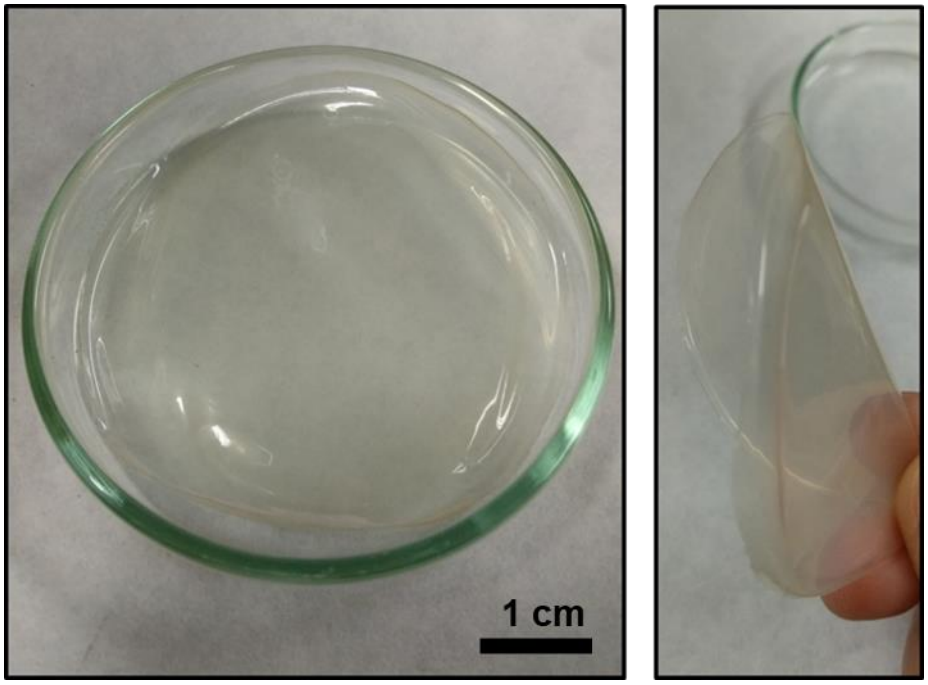

Figure 3: Image of the K@UPG-1_SPSU membrane

The proton conductivity of SPSU and K@UPG-1_SPSU were determined at different temperatures (from 40 ºC to 90 ºC) and 90% RH. As expected, the conductivity increases with the temperature (Fig. S31-34), reaching the maximum value at 90% RH and 80 ºC for both membranes ($9.57\ 10^{-3}$ and $8.51\ 10^{-3}$ $S \cdot cm^{-1}$ for SPSU and K@UPG-1_SPSU, respectively; see Figure 4).

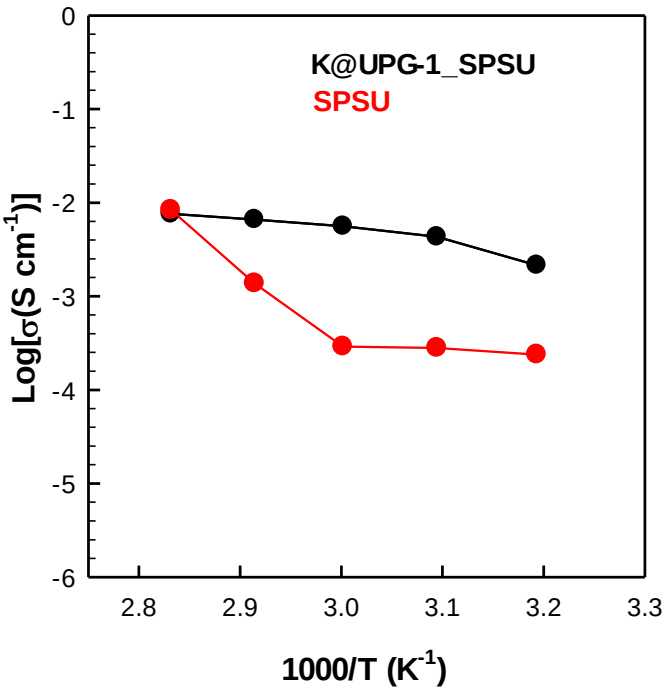

Figure 4: Evolution of the proton conductivity with temperature for SPSU and K@UPG-1_SPSU MMMs

The conductivity value obtained at high temperature for the MMM (80ºC; Figure 4) is within the range of the pure SPSU membrane, meanwhile its conductivity increases at lower temperatures. On the other hand, the increase of the conductivity, as well as the change of the slope of the pure polymeric membrane at high temperature (≥ 60ºC; Figure 4), are probably associated with an important hydration of the membrane due to its high sulfonic groups content, changing its proton conduction mechanism. In this sense, a higher content of sulfonic groups (DS) in a SPSU is associated to an important water absorption capacity (WU%), as reported by Martos *et al*.[52] In this work, the authors found a WU% at RT higher than 60% for SPSU with a DS of 77%. Although this hydration effect could lead to the membrane degradation, the incorporation of the MOF not only increases the conductivity at low temperatures but also enhances the membrane stability at high temperatures (as observed in the evolution of the proton conductivity with temperature and

macroscopically in absence of particle disaggregation). A similar behavior was previously described; both Morlanes *et al.* and Herrero *et al.* reported SPSU systems with different additives (*i.e.* SiO_2, SiO_2/phosphomolybdic, or layered double hydroxide at different proportions),[73,74] evidencing that an optimal percentage of nanoparticles can improve the proton conductivity of the membrane by reducing its water uptake and then, enhancing its stability.

In order to compare the conductivity mechanisms of the K@UPG-1 pellet and its K@UPG-1-SPSU membrane, the activation energy of the process was estimated for the MMM by fitting the conductivity data to the VTF equation (Fig. S34 and Table S6). Similarly to the value previously estimated for K@UPG-1 pellet, the E_a for K@UPG-1-SPSU was in the range of the Grotthuss mechanism. However, the difference between the pellet and the membrane values (0.059 and 0.004 eV, respectively) suggests a different conduction mechanism, as expected after the addition of the SPSU to shape the membrane.

On the whole, these preliminary data reveal that K@UPG-1_SPSU MMM exhibits a good proton conductivity with enhanced stability when compared with the pure SPSU membrane alone. Further optimization of the MOF loading in the membrane might lead to a higher proton conductivity, encouraging us to continue working on this approach in order to nearly use K@UPG-1_SPSU electrolytes in more efficient PEMs.

Conclusion

The ionic exchange of some labile protons (*ca*. 5 over 8 labile protons) from the UPG-1 by Li^+, Na^+ or K^+ was successfully achieved using a simple and fast wet method. The exchanged materials exhibited a water affinity higher than the pristine UPG-1, leading to enhanced conductivity values. Interestingly, the proton conductivity of the K-exchanged solid increased up to two magnitude

orders when compared with the pristine UPG-1 (from $5 \cdot 10^{-4}$ S·cm^{-1} to $2.3 \cdot 10^{-2}$ S·cm^{-1}), being among the highest reported values for phosphonate-MOFs. Further, its cyclability was assessed during three consecutive cycles, making the K@UPG-1 solid very promising as PEMFC electrolyte. Also, the successful loading of the K@UPG-1 into a MMM based on a sulfonated polysulfone led to a moderate proton conductivity ($8.51\ 10^{-3}$ S·cm^{-1}). Preliminary results demonstrated that the composites present a better mechanical stability than pressed powders, and enhanced properties (conductivity and stability) than membranes by incorporating just a 2 wt.% of MOF. Despite the moderate proton conductivity when compared with the literature or with the pristine material, the ion exchange strategy followed by the MMM shaping with proton conductivity values near to 10^{-2} S·cm^{-1} was carried out successfully. This strategy, combined with an optimization of the MOF loading into the membrane to reach higher conductivity values (>10^{-2} S·cm^{-1}) could guarantee the applications of these MOFs for fuel cell applications.

ASSOCIATED CONTENT

Supporting Information.

The following files are available free of charge. Snapshots from molecular simulation, PXRD patterns, FTIR spectra, TGA, Impedance spectra, Nyquist plots, Arrhenius plots, conductivity values, VTF fittings and parameters, SEM images, XEDS of the samples can be found at Supporting Information.

AUTHOR INFORMATION

Corresponding Author

*Patricia Horcajada. E-mail: patricia.horcajada@imdea.org.

*Alejandro Várez. E-mail: alvar@ing.uc3m.es

Author Contributions

The manuscript was written through contributions of all authors. All authors have given approval to the final version of the manuscript.

ACKNOWLEDGMENT

The authors acknowledge to the Ramón Areces Foundation project H+MOFs and to the M-ERA-NET C-MOF-cell project. The authors also thank the Agencia Española de Investigación /Fondo Europeo de Desarrollo Regional (FEDER/UE) for funding the projects PID2019-106662RBC43. This work has also been supported by Comunidad de Madrid (Spain) - multiannual agreement with UC3M ("Excelencia para el Profesorado Universitario" - EPUC3M04) - Fifth regional research plan 2016-2020.

REFERENCES

(1) Peighambardoust, S. J.; Rowshanzamir, S.; Amjadi, M. Review of the Proton Exchange Membranes for Fuel Cell Applications. *Int. J. Hydrogen Energy* **2010**, *35* (17), 9349–9384.

(2) Kraytsberg, A.; Ein-Eli, Y. Review of Advanced Materials for Proton Exchange Membrane Fuel Cells. *Energy Fuels* **2014**, *28* (12), 7303–7330.

(3) Yonoff, R. E.; Ochoa, G. V.; Cardenas-Escorcia, Y.; Silva-Ortega, J. I.; Meriño-Stand, L. Research Trends in Proton Exchange Membrane Fuel Cells during 2008–2018: A Bibliometric Analysis. *Heliyon* **2019**, *5* (5), e01724.

(4) Pollet, B. G.; Staffell, I.; Shang, J. L.; Molkov, V. Fuel-Cell (Hydrogen) Electric Hybrid Vehicles. In *Alternative Fuels and Advanced Vehicle Technologies for Improved Environmental Performance*; Elsevier, 2014; pp 685–735.

(5) Cannio, M.; Righi, S.; Santangelo, P. E.; Romagnoli, M.; Pedicini, R.; Carbone, A.; Gatto, I. Smart Catalyst Deposition by 3D Printing for Polymer Electrolyte Membrane Fuel Cell Manufacturing. *Renew. Energy* **2021**, *163*, 414–422.

(6) Han, C.; Chen, Z. Study on the Synergism of Thermal Transport and Electrochemical of PEMFC Based on N, P Co-Doped Graphene Substrate Electrode. *Energy* **2021**, *214*, 118808.

(7) Kuan, Y.-D.; Ke, T.-R.; Lyu, J.-L.; Sung, M.-F.; Do, J.-S. Development of a Current Collector with a Graphene Thin Film for a Proton Exchange Membrane Fuel Cell Module. *Molecules* **2020**, *25* (4), 955.

(8) Díaz, M.; Ortiz, A.; Ortiz, I. Progress in the Use of Ionic Liquids as Electrolyte Membranes in Fuel Cells. *J. Membr. Sci.* **2014**, *469*, 379–396.

(9) Zatoń, M.; Rozière, J.; Jones, D. J. Current Understanding of Chemical Degradation Mechanisms of Perfluorosulfonic Acid Membranes and Their Mitigation Strategies: A Review. *Sustain. Energy Fuels* **2017**, *1* (3), 409–438.

(10) Wang, G.; Yu, Y.; Liu, H.; Gong, C.; Wen, S.; Wang, X.; Tu, Z. Progress on Design and Development of Polymer Electrolyte Membrane Fuel Cell Systems for Vehicle Applications: A Review. *Fuel Process. Technol.* **2018**, *179*, 203–228.

(11) Escorihuela, J.; Narducci, R.; Compañ, V.; Costantino, F. Proton Conductivity of Composite Polyelectrolyte Membranes with Metal-Organic Frameworks for Fuel Cell Applications. *Adv. Mater. Interfaces* **2019**, *6* (2), 1801146.

(12) Shaari, N.; Kamarudin, S. K. Recent Advances in Additive-Enhanced Polymer Electrolyte Membrane Properties in Fuel Cell Applications: An Overview. *Int. J. Energy Res.* **2019**, *43* (7), 2756–2794.

(13) Zakil, F. A.; Kamarudin, S. K.; Basri, S. Modified Nafion Membranes for Direct Alcohol Fuel Cells: An Overview. *Renew. Sustain. Energy Rev.* **2016**, *65*, 841–852.

(14) Ramaswamy, P.; Wong, N. E.; Shimizu, G. K. H. MOFs as Proton Conductors – Challenges and Opportunities. *Chem. Soc. Rev.* **2014**, *43* (16), 5913–5932.

(15) Han, W.; Kwan, S. M.; Yeung, K. L. Zeolite Applications in Fuel Cells: Water Management and Proton Conductivity. *Chem. Eng. J.* **2012**, *187*, 367–371.

(16) Pornprasertsuk, R.; Kosasang, O.; Somroop, K.; Horprathum, M.; Limnonthakul, P.; Chindaudom, P.; Jinawath, S. Proton Conductivity of Y-Doped BaZrO3: Pellets and Thin Films. *Solid State Sci.* **2011**, *13*, 1429–1437.

(17) Abouzari-lotf, E.; Jacob, M. V.; Ghassemi, H.; Ahmad, A.; Nasef, M. M.; Zakeri, M.; Mehdipour-Ataei, S. Enhancement of Fuel Cell Performance with Less-Water Dependent Composite Membranes Having Polyoxometalate Anchored Nanofibrous Interlayer. *J. Power Sources* **2016**, *326*, 482–489.

(18) Montoro, C.; Rodríguez-San-Miguel, D.; Polo, E.; Escudero-Cid, R.; Ruiz-González, M.

L.; Navarro, J. A. R.; Ocón, P.; Zamora, F. Ionic Conductivity and Potential Application for Fuel Cell of a Modified Imine-Based Covalent Organic Framework. *J. Am. Chem. Soc.* **2017**, *139* (29), 10079–10086.

(19) Karim, M. R.; Hatakeyama, K.; Koinuma, M.; Hayami, S. Proton Conductors Produced by Chemical Modifications of Carbon Allotropes, Perovskites and Metal Organic Frameworks. *J. Mater. Chem. A* **2017**, *5* (16), 7243–7256.

(20) Wang, H.; Zhu, Q.-L.; Zou, R.; Xu, Q. Metal-Organic Frameworks for Energy Applications. *Chem* **2017**, *2*, 52–80.

(21) Sadakiyo, M.; Yamada, T.; Kitagawa, H. Hydrated Proton-Conductive Metal–Organic Frameworks. *Chempluschem* **2016**, *81* (8), 691–701.

(22) Li, A.; Gao, Q.; Xu, J.; Bu, X. Proton-Conductive Metal-Organic Frameworks: Recent Advances and Perspectives. *Coord. Chem. Rev.* **2017**, *344*, 54–82.

(23) Horike, S.; Umeyama, D.; Kitagawa, S. Ion Conductivity and Transport by Porous Coordination Polymers and Metal–Organic Frameworks. *Acc. Chem. Res.* **2013**, *46* (11), 2376–2384.

(24) Vilela, S. M. F.; Salcedo-Abraira, P.; Gómez-Peña, A.; Trens, P.; Várez, A.; Salles, F.; Horcajada, P. Proton Conductive Zr-Phosphonate UPG-1—Aminoacid Insertion as Proton Carrier Stabilizer. *Molecules* **2020**, *25* (15), 3519.

(25) Furukawa, H.; Cordova, K. E.; O'Keeffe, M.; Yaghi, O. M. The Chemistry and Applications of Metal-Organic Frameworks. *Science* **2013**, *341*, 974–986.

(26) Farha, O. K.; Eryazici, I.; Jeong, N. C.; Hauser, B. G.; Wilmer, C. E.; Sarjeant, A. A.; Snurr, R. Q.; Nguyen, S. T.; Yazaydın, A. Ö.; Hupp, J. T. Metal–Organic Framework Materials with Ultrahigh Surface Areas: Is the Sky the Limit? *J. Am. Chem. Soc.* **2012**, *134* (36), 15016–15021.

(27) Li, W.-H.; Deng, W.-H.; Wang, G.-E.; Xu, G. Conductive MOFs. *EnergyChem* **2020**, *2* (2), 100029.

(28) Chen, X.; Li, G. Proton Conductive Zr-Based MOFs. *Inorg. Chem. Front.* **2020**, *7* (19), 3765–3784.

(29) Shigematsu, A.; Yamada, T.; Kitagawa, H. Wide Control of Proton Conductivity in Porous Coordination Polymers. *J. Am. Chem. Soc.* **2011**, *133* (7), 2034–2036.

(30) Ramaswamy, P.; Matsuda, R.; Kosaka, W.; Akiyama, G.; Jeon, H. J.; Kitagawa, S. Highly Proton Conductive Nanoporous Coordination Polymers with Sulfonic Acid Groups on the Pore Surface. *Chem. Commun.* **2014**, *50* (9), 1144–1146.

(31) Yang, F.; Xu, G.; Dou, Y.; Wang, B.; Zhang, H.; Wu, H.; Zhou, W.; Li, J.-R.; Chen, B. A Flexible Metal–Organic Framework with a High Density of Sulfonic Acid Sites for Proton Conduction. *Nat. Energy* **2017**, No. 2, 877–883.

(32) Phang, W. J.; Jo, H.; Lee, W. R.; Song, J. H.; Yoo, K.; Kim, B.; Hong, C. S. Superprotonic Conductivity of a UiO-66 Framework Functionalized with Sulfonic Acid Groups by Facile Postsynthetic Oxidation. *Angew. Chemie Int. Ed.* **2015**, *54* (17), 5142–5146.

(33) Pardo, E.; Train, C.; Gontard, G.; Boubekeur, K.; Fabelo, O.; Liu, H.; Dkhil, B.; Lloret, F.;

Nakagawa, K.; Tokoro, H.; Ohkoshi, S.; Verdaguer, M. High Proton Conduction in a Chiral Ferromagnetic Metal–Organic Quartz-like Framework. *J. Am. Chem. Soc.* **2011**, *133* (39), 15328–15331.

(34) Sadakiyo, M.; Yamada, T.; Kitagawa, H. Rational Designs for Highly Proton-Conductive Metal−Organic Frameworks. *J. Am. Chem. Soc.* **2009**, *131* (29), 9906–9907.

(35) Liu, L.; Yao, Z.; Ye, Y.; Liu, C.; Lin, Q.; Chen, S.; Xiang, S.; Zhang, Z. Enhancement of Intrinsic Proton Conductivity and Aniline Sensitivity by Introducing Dye Molecules into the MOF Channel. *ACS Appl. Mater. Interfaces* **2019**, *11* (18), 16490–16495.

(36) Luo, H.-B.; Ren, Q.; Wang, P.; Zhang, J.; Wang, L.; Ren, X.-M. High Proton Conductivity Achieved by Encapsulation of Imidazole Molecules into Proton-Conducting MOF-808. *ACS Appl. Mater. Interfaces* **2019**, *11* (9), 9164–9171.

(37) Khatua, S.; Kumar Bar, A.; Konar, S. Tuning Proton Conductivity by Interstitial Guest Change in Size-Adjustable Nanopores of a Cu I -MOF: A Potential Platform for Versatile Proton Carriers. *Chem. - A Eur. J.* **2016**, *22* (45), 16277–16285.

(38) Bureekaew, S.; Horike, S.; Higuchi, M.; Mizuno, M.; Kawamura, T.; Tanaka, D.; Yanai, N.; Kitagawa, S. One-Dimensional Imidazole Aggregate in Aluminium Porous Coordination Polymers with High Proton Conductivity. *Nat. Mater.* **2009**, *8* (10), 831–836.

(39) Ponomareva, V. G.; Kovalenko, K. A.; Chupakhin, A. P.; Dybtsev, D. N.; Shutova, E. S.; Fedin, V. P. Imparting High Proton Conductivity to a Metal–Organic Framework Material by Controlled Acid Impregnation. *J. Am. Chem. Soc.* **2012**, *134* (38), 15640–15643.

(40) Wu, G.; Zhou, H.; Fu, Z.; Li, W.; Xiu, J.; Yao, M.; Li, Q.; Xu, G. MOF Nanosheet Reconstructed Two-Dimensional Bionic Nanochannel for Protonic Field-Effect Transistors. *Angew. Chemie Int. Ed.* **2021**, *60* (18), 9931–9935.

(41) Xue, W.; Deng, W.; Chen, H.; Liu, R.; Taylor, J. M.; Li, Y.; Wang, L.; Deng, Y.; Li, W.; Wen, Y.; Wang, G.; Wan, C.; Xu, G. MOF-Directed Synthesis of Crystalline Ionic Liquids with Enhanced Proton Conduction. *Angew. Chemie Int. Ed.* **2021**, *60* (3), 1290–1297.

(42) Vilela, S. M. F.; Navarro, J. A. R.; Barbosa, P.; Mendes, R. F.; Pérez-Sánchez, G.; Nowell, H.; Ananias, D.; Figueiredo, F.; Gomes, J. R. B.; Tomé, J. P. C.; Paz, F. A. A. Multifunctionality in an Ion-Exchanged Porous Metal–Organic Framework. *J. Am. Chem. Soc.* **2021**, *143* (3), 1365–1376.

(43) Gagnon, K. J.; Perry, H. P.; Clearfield, A. Conventional and Unconventional Metal–Organic Frameworks Based on Phosphonate Ligands: MOFs and UMOFs. *Chem. Rev.* **2012**, *112* (2), 1034–1054.

(44) Bazaga-García, M.; Salcedo, I. R.; Colodrero, R. M. P.; Xanthopoulos, K.; Villemin, D.; Stock, N.; López-González, M.; del Río, C.; Losilla, E. R.; Cabeza, A.; Demadis, K. D.; Olivera-Pastor, P. Layered Lanthanide Sulfophosphonates and Their Proton Conduction Properties in Membrane Electrode Assemblies. *Chem. Mater.* **2019**, *31* (23), 9625–9634.

(45) Katayama, Y.; Bentz, K. C.; Cohen, S. M. Defect-Free MOF-Based Mixed-Matrix Membranes Obtained by Corona Cross-Linking. *ACS Appl. Mater. Interfaces* **2019**, *11* (13), 13029–13037.

(46) Bi, X.; Zhang, Y.; Zhang, F.; Zhang, S.; Wang, Z.; Jin, J. MOF Nanosheet-Based Mixed

Matrix Membranes with Metal-Organic Coordination Interfacial Interaction for Gas Separation. *ACS Appl. Mater. Interfaces* **2020**, *12* (43), 49101–49110.

(47) Wang, S.; Li, P.; Fan, S.; Fang, Z.; Wang, X.; Li, Z.; Peng, X. A Unique Photoswitch: Intrinsic Photothermal Heating Induced Reversible Proton Conductivity of a HKUST-1 Membrane. *Dalt. Trans.* **2021**, *50* (8), 2731–2735.

(48) Hussain, S.; Deng, Z.; Khan, A.; Li, P.; Li, Z.; Fang, Z.; Wan, X.; Peng, X. Photothermal Responsive Ultrathin Cu-TCPP Nanosheets/Sulfonated Polystyrene Nanocomposite Photo-Switch Proton Conducting Membranes. *J. Memb. Sci.* **2021**, *620*, 118888.

(49) Bisht, S.; Balaguru, S.; Ramachandran, S. K.; Gangasalam, A.; Kweon, J. Proton Exchange Composite Membranes Comprising SiO2, Sulfonated SiO2, and Metal–Organic Frameworks Loaded in SPEEK Polymer for Fuel Cell Applications. *J. Appl. Polym. Sci.* **2021**, *138* (22), 50530.

(50) Wang, H.; Zhao, Y.; Shao, Z.; Xu, W.; Wu, Q.; Ding, X.; Hou, H. Proton Conduction of Nafion Hybrid Membranes Promoted by NH 3 -Modified Zn-MOF with Host–Guest Collaborative Hydrogen Bonds for H 2 /O 2 Fuel Cell Applications. *ACS Appl. Mater. Interfaces* **2021**, *13* (6), 7485–7497.

(51) Taddei, M.; Costantino, F.; Marmottini, F.; Comotti, A.; Sozzani, P.; Vivani, R. The First Route to Highly Stable Crystalline Microporous Zirconium Phosphonate Metal–Organic Frameworks. *Chem. Commun.* **2014**, *50* (94), 14831–14834.

(52) Martos, A. M.; Sanchez, J.-Y.; Várez, A.; Levenfeld, B. Electrochemical and Structural Characterization of Sulfonated Polysulfone. *Polym. Test.* **2015**, *45*, 185–193.

(53) Iojoiu, C.; Genova-Dimitrova, P.; Maréchal, M.; Sanchez, J.-Y. Chemical and Physicochemical Characterizations of Ionomers. *Electrochim. Acta* **2006**, *51* (23), 4789–4801.

(54) Zview 2 for Windows (Version 2.0), Scribner Assoc. Inc., V. U. Zview 2 for Windows (Version 2.0). Scribner Assoc. Inc., VA USA (2000). Zview 2 for Windows (Version 2.0).: Charlottesville 2000.

(55) Rappe, A. K.; Casewit, C. J.; Colwell, K. S.; Goddard, W. A.; Skiff, W. M. UFF, a Full Periodic Table Force Field for Molecular Mechanics and Molecular Dynamics Simulations. *J. Am. Chem. Soc.* **1992**, *114* (25), 10024–10035.

(56) Abascal, J. L. F.; Vega, C. A General Purpose Model for the Condensed Phases of Water: TIP4P/2005. *J. Chem. Phys.* **2005**, *123* (23), 234505.

(57) Frenkel, D.; Smit, B. *Understanding Molecular Simulation (Computational Science Series, Vol 1)*; Academic Press, 2001.

(58) Tominaka, S.; Cheetham, A. K. Intrinsic and Extrinsic Proton Conductivity in Metal-Organic Frameworks. *RSC Adv.* **2014**, *4* (97), 54382–54387.

(59) Fulcher, G. S. Analysis of Recent Measurements of the Viscosity of Glasses. *J. Am. Ceram. Soc.* **1992**, *75* (5), 1043–1055.

(60) Diederichsen, K. M.; Buss, H. G.; McCloskey, B. D. The Compensation Effect in the Vogel-Tammann-Fulcher (VTF) Equation for Polymer-Based Electrolytes. *Macromolecules* **2017**, *50* (10), 3831–3840.

(61) Ogawa, T.; Aonuma, T.; Tamaki, T.; Ohashi, H.; Ushiyama, H.; Yamashita, K.; Yamaguchi, T. The Proton Conduction Mechanism in a Material Consisting of Packed Acids. *Chem. Sci.* **2014**, *5* (12), 4878–4887.

(62) Gao, Y.; Broersen, R.; Hageman, W.; Yan, N.; Mittelmeijer-Hazeleger, M. C.; Rothenberg, G.; Tanase, S. High Proton Conductivity in Cyanide-Bridged Metal–Organic Frameworks: Understanding the Role of Water. *J. Mater. Chem. A* **2015**, *3* (44), 22347–22352.

(63) de Grotthuss, C. J. T. Memoir on the Decomposition of Water and of the Bodies That It Holds in Solution by Means of Galvanic Electricity. *Biochim. Biophys. Acta - Bioenerg.* **2006**, *1757* (8), 871–875.

(64) Allcock, H. R.; Phelps, M. V. B.; Barrett, E. W.; Pishko, M. V.; Koh, W. G. Ultraviolet Photolithographic Development of Polyphosphazene Hydrogel Microstructures for Potential Use in Microarray Biosensors. *Chem. Mater.* **2006**, *18* (3), 609–613.

(65) Taddei, M.; Shearan, S. J. I.; Donnadio, A.; Casciola, M.; Vivani, R.; Costantino, F. Investigating the Effect of Positional Isomerism on the Assembly of Zirconium Phosphonates Based on Tritopic Linkers. *Dalt. Trans.* **2020**, *49* (12), 3662–3666.

(66) Costantino, F.; Donnadio, A.; Casciola, M. Survey on the Phase Transitions and Their Effect on the Ion-Exchange and on the Proton-Conduction Properties of a Flexible and Robust Zr Phosphonate Coordination Polymer. *Inorg. Chem.* **2012**, *51* (12), 6992–7000.

(67) Cai, Z.-S.; Bao, S.-S.; Wang, X.-Z.; Hu, Z.; Zheng, L.-M. Multiple-Step Humidity-Induced Single-Crystal to Single-Crystal Transformations of a Cobalt Phosphonate: Structural and Proton Conductivity Studies. *Inorg. Chem.* **2016**, *55* (7), 3706–3712.

(68) Colodrero, R. M. P.; Angeli, G. K.; Bazaga-Garcia, M.; Olivera-Pastor, P.; Villemin, D.; Losilla, E. R.; Martos, E. Q.; Hix, G. B.; Aranda, M. A. G.; Demadis, K. D.; Cabeza, A. Structural Variability in Multifunctional Metal Xylenediaminetetraphosphonate Hybrids. *Inorg. Chem.* **2013**, *52* (15), 8770–8783.

(69) Taylor, J. M.; Mah, R. K.; Moudrakovski, I. L.; Ratcliffe, C. I.; Vaidhyanathan, R.; Shimizu, G. K. H. Facile Proton Conduction via Ordered Water Molecules in a Phosphonate Metal−Organic Framework. *J. Am. Chem. Soc.* **2010**, *132* (40), 14055–14057.

(70) Pili, S.; Argent, S. P.; Morris, C. G.; Rought, P.; García-Sakai, V.; Silverwood, I. P.; Easun, T. L.; Li, M.; Warren, M. R.; Murray, C. A.; Tang, C. C.; Yang, S.; Schröder, M. Proton Conduction in a Phosphonate-Based Metal–Organic Framework Mediated by Intrinsic "Free Diffusion inside a Sphere." *J. Am. Chem. Soc.* **2016**, *138* (20), 6352–6355.

(71) Kim, S.; Dawson, K. W.; Gelfand, B. S.; Taylor, J. M.; Shimizu, G. K. H. Enhancing Proton Conduction in a Metal–Organic Framework by Isomorphous Ligand Replacement. *J. Am. Chem. Soc.* **2013**, *135* (3), 963–966.

(72) Mendes, R. F.; Barbosa, P.; Domingues, E. M.; Silva, P.; Figueiredo, F.; Almeida Paz, F. A. Enhanced Proton Conductivity in a Layered Coordination Polymer. *Chem. Sci.* **2020**, *11* (24), 6305–6311.

(73) Martínez-Morlanes, M. J.; Martos, A. M.; Várez, A.; Levenfeld, B. Synthesis and Characterization of Novel Hybrid Polysulfone/Silica Membranes Doped with Phosphomolybdic Acid for Fuel Cell Applications. *J. Memb. Sci.* **2015**, *492*, 371–379.

(74) Herrero, M.; Martos, A. M.; Varez, A.; Galván, J. C.; Levenfeld, B. Synthesis and

Characterization of Polysulfone/Layered Double Hydroxides Nanocomposite Membranes for Fuel Cell Application. *Int. J. Hydrogen Energy* **2014**, *39* (8), 4016–4022.